ARCHIVES OF ELECTRICAL ENGINEERING VOL. 67(3), pp. 529–543 (2018)

DOI 10.24425/123661

Measurement accuracy verification of phasor measurement unit with dynamic phasor estimation

BARTLOMIEJ ARENDARSKI[1], STEFFEN RABE[2], WOLFRAM HEINEKEN[1], PRZEMYSLAW KOMARNICKI[1]

[1] *Fraunhofer Institute for Factory Operation and Automation*
Sandtorstrasse 22, 39106 Magdeburg, Germany

[2] *GridLab GmbH*
Mittelstrasse 7, 12529 Schoenefeld, Germany
e-mail: {bartlomiej.arendarski/wolfram.heineken/przemyslaw.komarnicki}@iff.fraunhofer.de, steffen.rabe@gridlab.de

(Received: 04.06.2018, revised: 25.06.2018)

Abstract: Power systems that are highly loaded, especially by a stochastic supply of renewables and the presence of storages, require dynamic measurements for their optimal control. Phasor measurement units (PMUs) can be used to capture electrical parameters of a power system. Standards on the PMU dynamic performance have been modified to incorporate their new dynamic mode of operation. This paper examines the PMU dynamic performance and proposes essential algorithms for measurement accuracy verification. Measurements of dynamic input signals, which vary in amplitude or frequency, were taken during automated tests of two PMUs. The test results are presented and expounded with further recommendation for the performance requirements. This paper also presents and examines applied testing procedures with relevance to the specifications of the IEEE Standard for Synchrophasor C37.118.1™-2011 and its amendment C37.118.1a™-2014.

Key words: discrete Fourier transform (DFT), dynamic phasor, measurement accuracy, phasor measurement unit (PMU), power system

1. Introduction

Assuring a reliable, continuous and safe supply of electricity is a main goal of the power supply. Changes in the electrical grid, its ongoing increasing of peak load, great penetration of renewable energy generation [1], use of mobile storage [2] are giving rise to increase the observability level in power systems. This requires effective and consistent gird monitoring and system state assessment [3], which can be supported by PMU technology [4].

Phasor measurement units, PMUs, constitute one option for capturing system parameters and have become established primarily in transmission grids. However, synchrophasors have

application possibilities in the distribution grids as well because the high accurate measurements of voltage, current, phase angle and frequency have many benefits for state estimation [5], adaptive protection and local control [4]. The phasor concept has been correspondingly expanded to detect changes in magnitude and phase by time. These changes can appear in the system as disturbances and produce discontinuous points such as step and ramp changes in voltage and current waveforms caused by electromagnetic transients [6].

PMU placement [7] and the accuracy of the measurements play the important role for different applications as fault location [8], temperature monitoring [9] or state estimation generally [10] or by incomplete observability [11], synchronous generator data identification [5] and other. Optimal placement of PMUs relates to the locations of installation and application in the system as well as to the defined total number of needed PMUs [12, 13].

Especially, attention is paid to the accuracy of measurements, which influence the fault tolerance and the exactness of the identified parameters, e.g. lines [14]. The improvement of dynamic behavior of the PMU makes it possible to increase the measuring exactness. Some authors discussed the specified method and set-ups for testing e.g. PMU dynamic performances, time accuracy measurement [15] or the answer of the PMU on the step signal [16]. More of these performance requirements have found place in the IEEE Synchrophasor Standard C37.118.1™-2011 [17] and its amendment C37.118.1a™-2014 [18].

Tendency for more communication in power systems (Smart Grids) using standardized protocols for both the communication e.g. IEC 61850 and smart grid equipment description, e.g. CIM, electric vehicles [19], is a promising prospect for the broad use of the PMU at all network levels [20]. The standard C37.118.2 ™-2011 defines the method for real-time exchange of synchronized phasor measurement data between power system equipment [21].

Standard fast Fourier transformation (FFT) cannot be used to evaluate dynamic signals in which the magnitude of the fundamental component of the signal changes within the window of analysis, because it does not deliver accurate results. To estimate the dynamic phasor a complex Taylor Fourier series is applied instead, as referred by [22], which allows for the approximation of dynamic signals. Further methods of dynamic phasor estimation are given by [23] and [24], which apply the weighted least square (WLS) approximation of a Taylor (WLST) signal model. Other authors present a new hybrid adaptive filter based on modified Gauss–Newton adaptive linear element (MGNA) for estimating the fundamental and harmonic phasors [25]. The method using a double suboptimal-scaling-factor adaptive strong tracking Kalman filter (DSTKF) to estimates the dynamic phasor is given by [26].

The standards [17, 18] address the boundary conditions for power signals in steady and dynamic states but do not provide method to realize the signals and calculate the error values.

This paper presents a theoretical method of dynamic phasor estimation and its application for practical realization. A dedicated test bench [27] was erected to verify the performance and accuracy of the measuring instruments, which works according to the comparative measurement principle. The investigations are focused on following issues: relation to the requirement of the IEEE standards, monitoring the dynamic power signal that changes in amplitude and frequency during the testing of the PMU, proposed estimation method for reference values of dynamic power signals, comparison of reference values with the PMU measurement values for the PMU error identification, time synchronization, results evaluation. This approach served as the basis for all tests (static and dynamic) performed on the automated test bench. According to the standard

[17] and its amendment [18] the following steady-state and dynamic scenarios with different investigation ranges were considered: signal frequency variation, signal magnitude variation, phase angle variation, harmonic distortion test, out-of-band interfering signal test (anti-aliasing test), magnitude modulation test, phase angle modulation test, linear frequency ramp, step changes (for amplitude/for angle).

2. Dynamic phasor estimation method

The method based on Taylor-Fourier transforms, introduced by [22–24], was applied to estimate the dynamic phasor of a given signal. Let us consider the signal $s(t)$ given in (1)

$$s(t) = a(t)\cos\left(\omega_0 t + \varphi(t)\right), \tag{1}$$

the amplitude $a(t)$ and phase angle $\varphi(t)$ of which may vary with time, whereas its frequency $\omega_0 = 2\pi f_0$ is constant and known. The dynamic phasor of signal $s(t)$ is the complex function

$$p(t) = a(t)e^{j\varphi(t)}. \tag{2}$$

If the phasor $p(t)$ is given, the signal $s(t)$ can be calculated using (3).

$$s(t) = \frac{1}{2}\left(p(t)e^{j\omega_0 t} + \overline{p}(t)e^{-j\omega_0 t}\right). \tag{3}$$

It has been assumed that the signal is sampled at discrete and equidistant time instants t_i with the sample time interval $\Delta t = t_i - t_{i-1}$. A time window $W_k = [t_k - T/2,\, t_k + T/2]$ is defined in which the interval length is $T = 2N\Delta t$. The signal values $s(t_i)$ with $t_i \in W_k$ are used to estimate the phasor $p(t_k)$ at the interval center. In order to shorten the notation, phasor estimation is specified in a zero-centered window $[-T/2,\, T/2]$ and the time instants within the window are denoted by $t_{-N}, \ldots, t_N$ with $t_k = \dfrac{kT}{2N}$ for $k = -N, \ldots, N$. Since the method does not depend on the position of the window, it can be extended to arbitrary windows in an obvious manner.

The dynamic phasor is approximated by the quadratic formula given in (4).

$$p(t) = p_0 + p_1 t + p_2 t^2, \tag{4}$$

with the coefficients $p_0, p_1, p_2 \in \mathbb{C}$, where p_0 is the estimated phasor, p_1 is its first derivative and p_2 is its second derivative. Incorporating this formula in (3) results as (5).

$$s(t_k) = \frac{1}{2}\left((p_0 + p_1 t_k + p_2 t_k^2)e^{j\omega_0 t_k} + \left(\overline{p}_0 + \overline{p}_1 t_k + \overline{p}_2 t_k^2\right)e^{-j\omega_0 t_k}\right), \quad k = -N, \ldots, N. \tag{5}$$

Equation (5) can be written in matrix form as (6):

$$\boldsymbol{Bp} = \boldsymbol{s}, \tag{6}$$

with the following matrix and vector definitions:

– $\boldsymbol{B} = (b_{i,k})$ is a matrix of dimension $(2N+1) \times 6$ with the elements given in (7).

$$\begin{gathered} b_{i,1} = t_i^2 e^{j\omega_0 t_i}, \qquad b_{i,2} = t_i e^{j\omega_0 t_i}, \qquad b_{i,3} = e^{j\omega_0 t_i}, \qquad b_{i,4} = e^{-j\omega_0 t_i}, \\ b_{i,5} = t_i e^{-j\omega_0 t_i}, \qquad b_{i,6} = t_i^2 e^{-j\omega_0 t_i}, \qquad i = -N, \ldots, N, \end{gathered} \tag{7}$$

– The vectors $\boldsymbol{s}$ and $\boldsymbol{p}$ are given by

$$\boldsymbol{s} = (s(t_{-N}), \ldots, s(t_k), \ldots, s(t_N))^T \qquad \text{and} \qquad (\boldsymbol{p} = p_2, p_1, p_0, \overline{p}_0, \overline{p}_1, \overline{p}_2)^T.$$

Equation (6) is an over-determined linear system for the three unknowns p_0, p_1 and p_2 which, in general, does not have a solution. A least-squares approximation is provided by (8).

$$\widehat{p} = (\boldsymbol{B}^H \boldsymbol{B})^{-1} \boldsymbol{B}^H \boldsymbol{s}, \tag{8}$$

where H is the Hermitian transpose operator, i.e. $\boldsymbol{B}^H = \boldsymbol{B}^T$. The matrix $\boldsymbol{B}^+ = (\boldsymbol{B}^H \boldsymbol{B})^{-1} \boldsymbol{B}^H$ is called the pseudo-inverse of $\boldsymbol{B}$. The solution vector $\widehat{p}$ has the form given in (9).

$$\widehat{p} = \left(\widehat{p}_2, \widehat{p}_1, \widehat{p}_0, \overline{\widehat{p}_0}, \overline{\widehat{p}_1}, \overline{\widehat{p}_2}\right)^T. \tag{9}$$

In keeping with formula (4), the phasor at the interval center is $p(0) = p_0$. Since $\widehat{p}_0$ is an approximation of p_0, it is taken as the phasor estimate. Furthermore, the following estimates can also be derived at the interval center $t = 0$:

– the amplitude $a(0) = |p(0)| = |p_0|$ is estimated by $\widehat{a} := |\widehat{p}_0|$,
– the phase angle $\varphi(0) = \arg(p(0)) = \arg(p_0)$ is estimated by $\widehat{\varphi} := \arg(\widehat{p}_0)$,
– the derivative of the phase angle $\varphi'(0) = \dfrac{1}{a(0)} \mathrm{Im}\left(p_1(0) e^{-j\varphi(0)}\right)$ can be estimate by $\widehat{\varphi}' = \dfrac{1}{\widehat{a}} \mathrm{Im}\left(\widehat{p}_1 e^{-j\widehat{\varphi}}\right)$.

The derivative of the phase angle can also be approximated by the difference quotient of the phase angle estimate $\widehat{\varphi}$. When the method is applied, it is preferable to use the difference quotient of $\widehat{\varphi}$ since it appears to yield more accurate results.

The derivative of the phase angle is of particular interest since it can be used to estimate the frequency of the signal. The signal $s(t)$ is given in phase modulation form in Equation (1). Phase modulation can also be interpreted as frequency modulation with the frequency $\omega(t) = \omega_0 + \varphi'(t)$. Therefore, $\widehat{\omega} := \omega_0 + \widehat{\varphi}'$ can be understood as an estimate of the frequency $\omega(t)$ at time $t = 0$.

3. Error estimation for PMU data

Let us consider a three phases signal given in (10),

$$\begin{aligned} s^{(1)}(t) &= a(t) \cos(\omega_0 t + \varphi(t)), \\ s^{(2)}(t) &= a(t) \cos(\omega_0 t + \varphi(t) + 2\pi/3), \\ s^{(3)}(t) &= a(t) \cos(\omega_0 t + \varphi(t) + 4\pi/3), \end{aligned} \tag{10}$$

where s could stand for voltage or current. A reference signal $s_{\mathrm{ref}}^{(n)}(t)$, $n = 1, 2, 3$ is practically created which is aimed to reproduce the exact signal $s^{(n)}(t)$, but due to the presence of error, $s_{\mathrm{ref}}^{(n)}(t)$ is only an approximation to $s^{(n)}(t)$. The generated signal is measured by a PMU at times $t = iT$ for $i = 0, 1, 2, \ldots, m$. The PMU data consists of:

– amplitude values $a^{(n)}_{\mathrm{PMU},i} \approx a(iT)$ for $n = 1, 2, 3$,
– phase angle values $\varphi^{(1)}_{\mathrm{PMU},i} \approx \varphi(iT)$, $\varphi^{(2)}_{\mathrm{PMU},i} \approx \varphi(iT) + \frac{2\pi}{3}$, $\varphi^{(3)}_{\mathrm{PMU},i} \approx \varphi(iT) + \frac{4\pi}{3}$,
– and frequency values $f_{\mathrm{PMU},i} \approx f_0 + \frac{1}{2\pi}\varphi'(iT)$.

Thus, the phasor measured by the PMU is given by (11).

$$p^{(n)}_{\mathrm{PMU},i} = a^{(n)}_{\mathrm{PMU},i} \exp(j\varphi^{(n)}_{\mathrm{PMU},i}). \tag{11}$$

The reference signal $s^{(n)}_{\mathrm{ref}\,f}(t)$ is tabulated at times $t = k\Delta t - T/2$ for

$$k = 0, 1, 2, \ldots, 2N(m+1),$$

where $\Delta t = T/(2N)$.

Let the tabulated values be denoted by $s^{(n)}_{\mathrm{ref}\,f,k} = s^{(n)}_{\mathrm{ref}\,f}(k\Delta t - T/2)$.

The following values were chosen for this analysis:

$$f_0 = 50\ \mathrm{Hz}, \qquad \omega_0 = 2\pi \cdot 50\ \mathrm{Hz}, \qquad T = 0.04\ \mathrm{s}, \qquad \Delta t = 10^{-5}\ \mathrm{s}, \qquad N = 2000.$$

The following PMU measurement errors are defined with respect to the reference signal:

– relative amplitude error (12)

$$AE_i = \frac{\left|p^{\Sigma}_{\mathrm{PMU},i}\right| - \left|p^{\Sigma}_{\mathrm{ref}\,f,i}\right|}{\left|p^{\Sigma}_{\mathrm{ref}\,f,i}\right|}, \tag{12}$$

– absolute phase error (13)

$$PE_i = \left|\arg\left(p^{\Sigma}_{\mathrm{PMU},i}\right) - \arg\left(p^{\Sigma}_{\mathrm{ref}\,f,i}\right)\right|, \tag{13}$$

– total vector error (14)

$$TVE_i = \frac{\left|p^{\Sigma}_{\mathrm{PMU},i} - p^{\Sigma}_{\mathrm{ref}\,f,i}\right|}{\left|p^{\Sigma}_{\mathrm{ref}\,f,i}\right|}, \tag{14}$$

– frequency error (15)

$$FE_i = f_{\mathrm{PMU},i} - \frac{f^{(1)}_{\mathrm{ref}\,f,i} + f^{(2)}_{\mathrm{ref}\,f,i} + f^{(3)}_{\mathrm{ref}\,f,i}}{3}, \tag{15}$$

where $p^{\Sigma}_{\mathrm{ref}\,f,i}$ and $p^{\Sigma}_{\mathrm{PMU},i}$ are the sums of phase-shifted phasors according to (16) and (17):

$$p^{\Sigma}_{\mathrm{ref}\,f,i} = p^{(1)}_{\mathrm{ref}\,f,i} + p^{(2)}_{\mathrm{ref}\,f,i} e^{-2\pi j/3} + p^{(3)}_{\mathrm{ref}\,f,i} e^{-4\pi j/3}, \tag{16}$$

$$p^{\Sigma}_{\mathrm{PMU},i} = p^{(1)}_{\mathrm{PMU},i} + p^{(2)}_{\mathrm{PMU},i} e^{-2\pi j/3} + p^{(3)}_{\mathrm{PMU},i} e^{-4\pi j/3}. \tag{17}$$

If only one phase is considered, then the total vector error takes the form given in (18):

$$TVE^{(1)}_i = \frac{\left|p^{(1)}_{\mathrm{PMU},i} - p^{(1)}_{\mathrm{ref}\,f,i}\right|}{p^{(1)}_{\mathrm{ref}\,f,i}}. \tag{18}$$

This corresponds to the formula given in the standard (IEEE C37.118.1, 2011), where the amplitude and phase differences are considered together, like presented in (19):

$$TVE(n) = \sqrt{\frac{\left(\widehat{X}_r(n) - X_r(n)\right)^2 + \left(\widehat{X}_i(n) - X_i(n)\right)^2}{(X_r(n))^2 + (X_i(n))^2}}, \tag{19}$$

where $\widehat{X}_r(n)$ and $\widehat{X}_i(n)$ are the sequences of estimates from the tested unit, and $X_r(n)$ and $X_i(n)$ are the sequences of theoretical values of the input signal at the instants of time (n) assigned to those values by the unit.

4. PMU accuracy assessment

4.1. Automated test bench

The proposed algorithm was implemented in the developed and certified test bench to verify the accuracy of devices under test (DUT). The test bench, its components and functionality are described in detail by [27].

The measuring system provides two ways of data acquisition (DAQ), see Fig. 1. First way is a direct feeding of current and voltage signals for DUT, which is realized for the measurement purposes and provides the PMU measurement data. Second path provides the signals, which are recorded by a reference measurement (REF) device, in parallel. This will allow a direct comparison of the measured data with the reference values and their further evaluation because of the GPS-based time synchronization of the test bench.

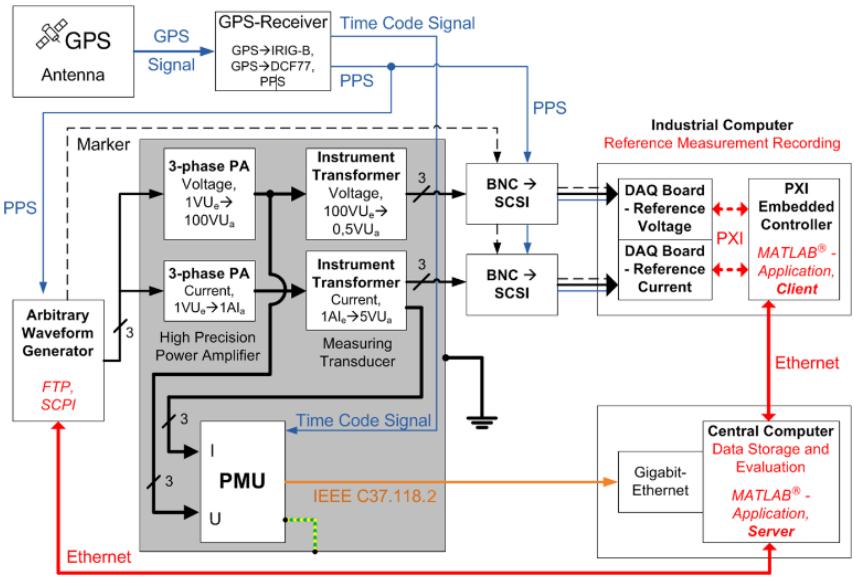

Fig. 1. Block diagram of the automated PMU test bench by [27]

An arbitrary waveform generator (AWG), which can perform any complex output signals and test sequences, is responsible for the input signals.

To provide real field conditions for the working PMU unit, the generated signal is amplified to the dimensions of conventional instrument transformers (e.g. 100 V/1 A interface). The amplification of the three-phase signal is realized by linear precision power amplifiers (PA), for both voltage and current. However, the signal level for the reference measurement device has to be reduced again, because the DAQ boards work in the range of extra-low voltage. This is realized by the measurement transducers.

The reference signal recorded by the DAQ is considered as a working standard to which the PMU measured signal is compared. Therefore, the reference measuring equipment is calibrated with a highly accurate, calibrated digital multi-meter. RMS measurement with a multi-meter for a voltage and current test signal is performed at the output of the transducer. In parallel this test signal is recorded with the DAQ boards to determine a correction factor for the later reference measurements. The data acquisition boards are connected to the controller by PCI eXtensions for Instrumentation (PXI), a modular electronic instrumentation platform for attaching hardware devices to a local computer bus. A digital marker signal provided by the AWG is used as a trigger source.

To ensure comparison of exactly the same time frame from the PMU and reference measurements, a highly accurate GPS time source is used for generating the TTL – time synchronization signals (pulse per second – PPS) with a pulse length of 200 ms for the test bench. A number of test bench features are presented in Table 1.

Table 1. Selected PMU test bench features by 0

Device	**Features**		
GPS receiver	Synchronization type	PPS	
	Synchronization accuracy	≤ 1 µs	
Arbitrary Waveform Generator	Output voltage	-5 V. . . +5 V	
	Sample rate	Up to 200 MS/s	
	Resolution of D/A converter	16 bit	
3-Phase high precision power amplifier		Voltage	Current
	Parameter	±400 V/±1.5 A	±10 A or ±2 A/±5 V
	Dynamics (bandwidth)	DC. . . 30 kHz (−3 dB)	
Transducer		Voltage	Current
	Transducer accuracy	±2.5%	±0.25%
	Transducer bandwidth	20 MHz	500 kHz
DAQ boards		Voltage	Current
	Sample rate	Up to 250 kS/s	Up to 1 MS/s
	Input voltage range	±5 V	±10 V
	Resolution of A/D converter	16 bit	

Data from the tested PMUs were recorded under European nominal frequency conditions of 50 Hz with a reporting rate of 25 frames per second. Test scenarios can be created by using numeric formula expressions in generated equation files to describe output waveform or by generating directly executable waveform files. This file format contains single-precision floating point numbers in 4-byte little-endian format in keeping with the standard IEEE 488.2 as well as specifications for the markers.

4.2. Application on a test signal

The IEEE standard [17, 18] provides a definition and limits for power signals under steady and dynamic conditions. The standard defines that the TVE, FE, and RFE for each performance requirement shall be the average, rms, or maximum value observed over a minimum of 5 s of test duration. The specific methodology for the signals and the test sequences are not given in the standard. Certain assumptions were therefore adopted for purposes of measurement, namely a measurement window of 10 s and 25 phasors per second.

The data sets of measured voltage and current are processed separately to evaluate the measurement. The evaluation starts with detection of the exact beginning of the respective seconds within the PMU raw measurement. The existence of records is checked within the particular seconds by a comparison with a minimum amplitude value. To ensure the correct quality of the phasors data, the first and last 25 phasors of the 250 that were taken in a 10 s measurement window are cut. In parallel, preparations of the reference measurement data sets are performed. The number of PPS signals corresponds to the 10 s duration of recording. To ensure the correct number of sample values (according to the preset DAQ board sample rate) a counting test between the first and last positive PPS signal slope is realized. A correction algorithm is implemented whenever there is any deviation. Therefore, a new time vector is created with correct time steps, which is applied to the cut reference measurement data set. This interpolation algorithm calculates the proper and corresponding sample values.

The dynamic phasor estimation method described in sections 2 and 3 was applied to a reference three-phase voltage signal. The signal is given in a time interval of 8 s. It has a frequency of 50 Hz and it is phase modulated with 0.2 Hz. The signal has been scaled to allow for the calibration of the PMU described in section 4.1. A four-second section of the first phase is presented in Fig. 2(a).

The algorithm is applied to the reference signal $s^{(n)}_{\mathrm{ref}\,f,i}$, resulting in amplitude values $a^{(n)}_{\mathrm{ref}\,f,i} = \left|p^{(n)}_{\mathrm{ref}\,f,i}\right|$, and phase angle values $\varphi^{(n)}_{\mathrm{ref}\,f,i} = \arg(p^{(n)}_{\mathrm{ref}\,f,i})$, where the index $n = 1, 2, 3$ corresponds to the phase and the index i corresponds to the time instant $t_i = iT$ with $T = 0.04$ s. The PMU measurements result in amplitude $a^{(n)}_{\mathrm{PMU},i}$ and phase values $\varphi^{(n)}_{\mathrm{PMU},i}$.

The errors of the PMU measurements of the test signal are defined in (8), (9), (10) and (11). Exemplary demonstration of the total vector error is shown in Fig. 2(b).

Because the error varies with time (solid blue line) over the time interval of the signal, the mean value (dashed red line) is also indicated in the plot. To evaluate the selected test results, the mean values are taken to represent the changes in error as point values in the analyzed scenarios (e.g. Fig. 3(a,b)).

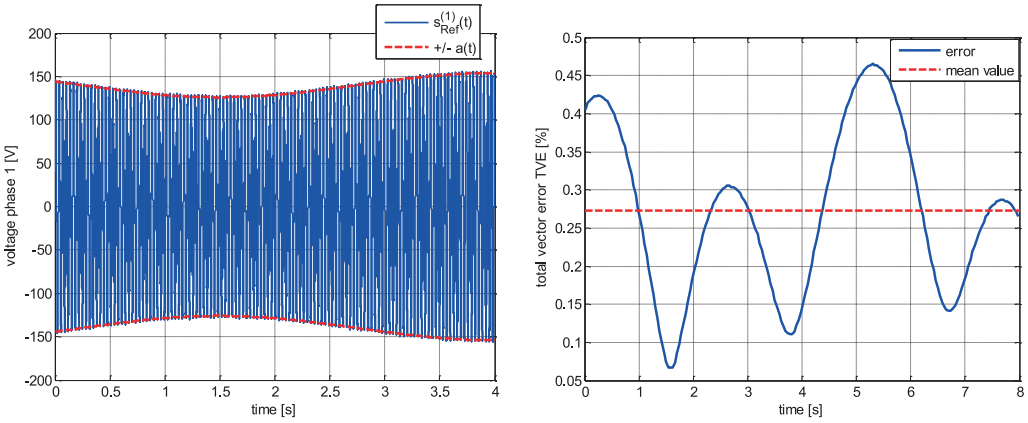

(a) (b)

Fig. 2. Reference signal, first phase (a), total vector error (b)

5. Practical test results

5.1. Test scenarios according IEEE Std C37.118.1aTM – 2014

In keeping with the standard steady state, scenarios are divided into signal frequency variation, signal magnitude variation, phase angle variation, harmonic distortion, and out-of-band interference signal (anti-aliasing). The corresponding dynamic compliance test scenarios are magnitude modulation, angle modulation, linear frequency ramp, and step changes (for amplitude/for angle).

All tests are performed phase symmetrical, which means that all three phases were always considered/changed equally; the changes were not made, for example, in only one phase. The average ambient temperature of the PMUs during the tests was 23.9°C.

Two PMUs from different manufacturers were tested in parallel and denoted as PMU A and PMU B, respectively.

The amplitude error (AE), phase error (PE), frequency error (FE) and total vector error (TVE) are identified for each scenario (apart from step change). The error calculation method is presented in sections 3 and 4.2. This study only discusses select errors in each scenario. Measurements were always performed for voltage and current, respectively.

5.2. Phase angle modulation test

The phase angle signal is modulated in this test scenario with settings presented in Table 2.

IEEE Std C37.118.1a^{TM} – 2014 defines two evaluation criteria for PMUs depending on the performance of devices for Protection (P) class and/or Measurement (M) class. This study considers the performance of M class to be the more demanding of the two. Table 3 presents the modulation test compliance requirements.

Table 2. Scenario definitions for modulation tests

	Class M
Amplitude of fundamental component	100 V/1 A
Frequency of fundamental component	50 Hz
Tested modulation frequencies [Hz]	0.2, 0.6, 1.0, 1.4, 1.8, 2.2, 2.6, 3.0, 3.4, 3.8, 4.2, 4.6, 4.8

Table 3. Modulated test compliance requirements

Modulation level	**Reference condition**	**Performance class M**	
		Range	Limit
$k_x = 0.1$, $k_a = 0$ rad	100% rated signal magnitude, f_{nominal}	Modulation frequency 0.1 to lesser of $F_s/5$ Hz or 5 Hz	MaxTVE: 3% MaxFE: 0.30 Hz MaxRFE: 14 Hz/s
$k_x = 0$, $k_a = 0.1$ rad			

The accuracy results are presented in Fig. 3(a,b) as average error values for each frequency in the range of 0.2–4.8 Hz. To ensure data validity the first and last second of the measurement are cut off for the parameter calculation, and thus 200 phasors are compared.

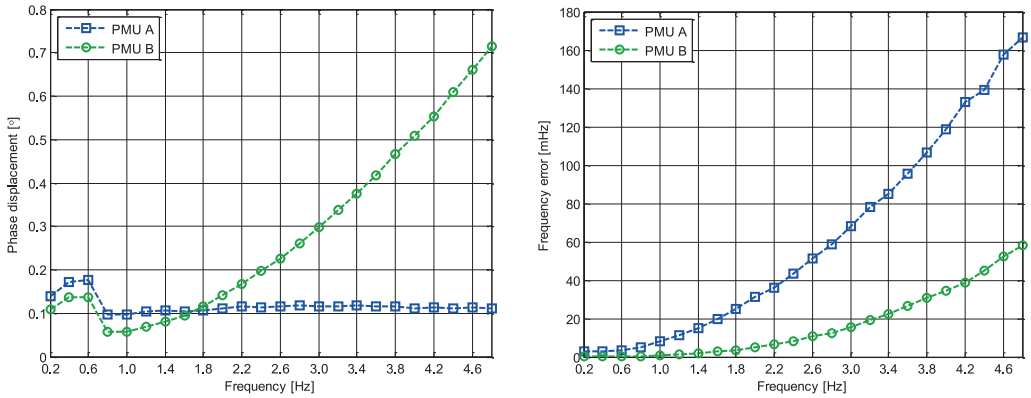

(a) (b)

Fig. 3. Phase angle modulation (voltage): phase displacement error (a); frequency error (b)

The phase error is calculated with Equation (9) for all investigated frequencies, respectively. Phase errors of PMU A (blue curve with squares) are lower than 0.2°and for PMU B (green curve with circles) they reach over 0.7°in the measured range (see Fig. 3(a)).

The frequency error, calculated with (11), is higher for PMU A and approaches over 160 mHz, whereas the frequency error for PMU B reaches 60 mHz (see Fig. 3(b)). The internal algorithms implemented in the respective device can cause this.

5.3. Linear frequency ramp

In the linear frequency ramp test a positive change of frequency from 50 Hz to 55 Hz with a ramp rate of 1 Hz per second was performed. The measurement duration was 5 seconds. The additional requirements are presented in Table 4. The evaluation criteria for these tests in keeping with C37.118.1a are specified in Table 5.

Table 4. Linear positive frequency ramp scenario definitions

	Class M
Amplitude of fundamental component	100 V/1 A
Frequency of fundamental component	50 Hz
Change of frequency	1 Hz/s (50 Hz → 55 Hz)

Table 5. Linear frequency ramp test requirements

Reference condition		**Ramp range**	**Limit**
100% rated signal magnitude, and f_{nominal} at non-excluded point during the test	Class M	Lesser of $\pm(F_s/5)$ or ±5 Hz*	MaxTVE: 1% MaxFE: 0.01 Hz MaxRFE: 0.2 Hz/s

* for F_s = 12 FPS, ramp range shall be ±2 1/3 (two and one-third) Hz to allow for an integer number of samples in result

Exemplary errors of linear positive frequency ramp signal of voltage are presented. The total vector error is calculated with Equation (10) and presented in Fig. 4(a). The error of PMU A ranges between 0.08 and 0.2% (blue waveform with squares) and is below the 1% limit. The error of PMU B (green curve with circles) reaches values of 3.6% and exceeds the limit.

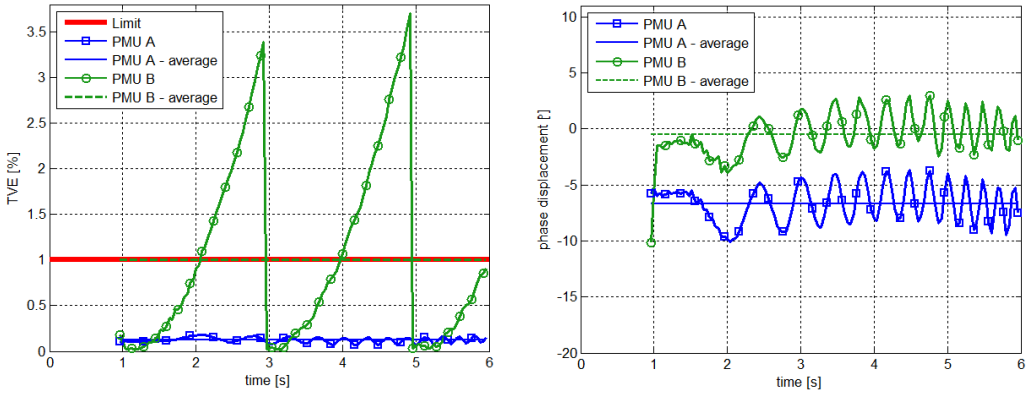

(a) (b)

Fig. 4. Linear positive frequency ramp (voltage): TVE error (a), phase error (b)

The phase errors are calculated with Equation (9), and the results are presented in Fig. 4(b). The errors of both PMUs have a similar waveform character. PMU B has smaller errors, except for the error at the beginning of the measurements which reaches $-10°$. The average phase error is $-6.5°$ for PMU A and $-0.6°$ for PMU B.

5.4. Step change scenario

The step change signal delay time was tested for the final dynamic behavior. Selected requirements and evaluation criteria for the step change scenario are presented in Table 6. It includes specifications for amplitude and phase step change such as maximum response time, response delay, overshoot and frequency measurement response time. The reference condition is that all test settings are nominal at the starting point. Readers are referred to standard (IEEE C37.118.1a, 2014) for other performance class M specifications.

Table 6. Step change test requirements

Step change specification	**Performance class M**	
	|Delay time (s)|	Max overshoot/undershoot
Magnitude = ±10%, $k_x = \pm 0.1$, $k_a = 0$	$1/(4 * F_s)$	10% of step magnitude
Angle ±10°, $k_x = 0$, $k_a = \pm\pi/18$	$1/(4 * F_s)$	10% of step magnitude

The results of the positive amplitude step changes of voltage measurements for the tested devices are presented in Fig. 5. The input signal magnitude was changed by +10%. Delay time is calculated from the contingent $1/(4 * F_s)$, whereby F_s is the reporting rate. It was set to 25 frames per second in this test.

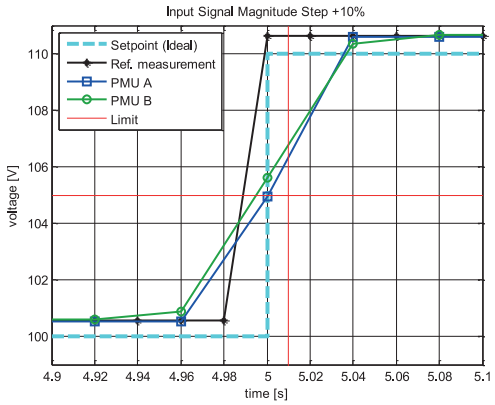

Fig. 5. Positive amplitude step change (voltage)

The stepped parameter should reach a value halfway between the start and end of the step change signal and, in this case, should be recorded in less than 10 ms. The delay time for both tested devices is under the limit. The beginning of the step change in relation to the signal time influences the result. In this case, it is always at the beginning of the second ($t = 0$), but it can

also be started in between. For that case the errors could be smaller, so the worst case (change of the second) was chosen.

The potential influence of different reporting rates on the step change response of PMUs was investigated. A change in the reporting rate (F_s = 10 and 50) does not affect the simulation (sequence accuracy) of an amplitude step change.

6. Conclusion

Consistent and secure smart grid system operation can be enhanced by the use of reliable and highly precise electric parameter measuring devices. These measurement results can be processed further for monitoring, control and protection issues.

The synchrophasor technology has many potential uses in applications where continuous network monitoring is needed and rapid decision-making in the event of a threat to the stability of the system is required. Changes in power grids, e.g. growth of decentralized energy generation, increase the dynamic behavior of the system. Especially, due to the tight coupling and relatively short distances between buses in distribution systems, the phase angles are closer and therefore the performance requirements would be more stringent for distribution class PMUs. Therefore, dynamic tests for measuring devices that work in these grids are needed.

In keeping with the standard (IEEE C37.118.1a, 2014) dynamic PMU measurement accuracy tests were performed and evaluated. New testing scenarios, corresponding to the smart grid operation conditions today and in the future, were discussed and applied to implement realistic operating conditions of PMUs. An existing test bench, and especially the software application, has been upgraded to handle the dynamic tests properly. A suitable estimation method was proposed, which detects changes in magnitude and phase according to the time during the transient period. The algorithm based on Taylor-Fourier transformations for dynamic phasor approximation was implemented in the test bench.

Comparison of the achieved tests' results shows that the PMUs can be used for dynamic measurements although in some cases their internal algorithms need to be improved.

References

[1] Buchholz B.M., Styczynski Z., *Smart grids – Fundamentals and technologies in electricity networks*, Springer (2014).

[2] Styczynski Z., Stoetzer M., Mueller G., Komarnicki P., Belmans R., Driesen J., Hansen A.B., Pecas Lopes J., Hatziargyriou N., *Challenges and barriers of integrating e-cars into a grid with high amount of renewable generation*, 44th International Conference on Large High Voltage Electric Systems (2012).

[3] Powalko M., Rudion K., Komarnicki P., Blumschein J., *Observability of the distribution system*, IET Conference Publications (2009).

[4] Phadke A.G., Thorp J.S., *Synchronized Phasor Measurements and Their Applications*, New York, Springer (2008).

[5] Wang X., Bialek J., Turitsyn K., *PMU-Based Estimation of Dynamic State Jacobian Matrix and Dynamic System State Matrix in Ambient Conditions*, IEEE Transactions on Power Systems, DOI 10.1109/TPWRS.2017.2712762.

[6] Ren J., *Synchrophasor measurement using substation intelligent electronic devices: algorithms and test methodology*, PhD Thesis, Office of Graduate Studies, Texas A&M University (2011).

[7] Richter M., *PMU-basierte Zustandsabschätzung in Smart Distribution*, PhD Thesis, EIT Faculty, Otto von Guericke University Magdeburg (2016).

[8] Al-Mahammed A.H., Abido M.A., *An adaptive fault location algorithm for power system networks based on synchrophasor measurements*, Electric Power System Research, vol. 108, pp. 153–163 (2014).

[9] Du Y., Liao Y., *On-line estimation of transmission line parameters, temperature and sag using PMU measurements*, Electric Power Systems Research, vol. 93, pp. 39–45 (2012).

[10] Guo Y., Wu W., Zhang B., Sun H., *A distributed state estimation method for power systems incorporating linear and nonlinear models*, International Journal of Electrical Power and Energy Systems, 64, pp. 608–616 (2015).

[11] Kashyap N., Werner S., Huang Y.-F., Riihonen T., *Power system state estimation under incomplete PMU observability – A reduced-order approach*, IEEE Journal on Selected Topics in Signal Processing, vol. 8, no. 6, art. 6845308, pp. 1051–1062 (2014).

[12] Yuill W., Edwards A., Chowdhury S., Chowdhury S.P., *Optimal PMU placement: A comprehensive literature review*, IEEE Power and Energy Society General Meeting, art. 6039376 (2011).

[13] Mueller G., Komarnicki P., Golub I., Styczynski Z., Dzienis C., Blumschein J., *PMU placement method based on decoupled newton power flow and sensitivity analysis*, 9th International Conference on Electrical Power Quality and Utilisation, art. 4424116 (2007).

[14] Chen C., Wang J., Zhu H., *Effects of phasor measurement uncertainty on power line outage detection*, IEEE Journal on Selected Topics in Signal Processing, vol. 8, no. 6, art. 6846291, pp. 1127–1139 (2014).

[15] Komarnicki P., Dzienis C., Styczynski Z.A., Blumschein J., Centeno V., *Practical experience with PMU system testing and calibration requirements*, IEEE Power and Energy Society 2008 General Meeting, PES, art. 4596629 (2008).

[16] Ren J., Kezunovic M., Stenbakken G., *Characterizing dynamic behavior of PMUs using step signals*, European Transactions on Electrical Power, 21 (4), pp. 1496–1508 (2011).

[17] IEEE Standard for Synchrophasor Measurements for Power Systems, (IEEE Std C37.118.1™-2011, revision of IEEE Std C37.118™-2005), December 2011.

[18] IEEE Standard for Synchrophasor Measurements for Power Systems (IEEE Std C37.118.1a™-2014 Amendment 1: Modification of Selected Performance Requirements, amendment to IEEE Std C37.118.1™-2011), March 2014.

[19] Heuer J., Komarnicki P., Styczynski Z.A., *Integration of electrical vehicles into the smart grid in the Harz.EE-mobility research project*, IEEE Power and Energy Society General Meeting, art. no. 6039147 (2011).

[20] Naumann A., Bielchev I., Voropai N., Styczynski Z., *Smart grid automation using IEC 61850 and CIM standards*, Control Engineering Practice, 25 (1), pp. 102–111 (2014).

[21] IEEE Standard for Synchrophasor Data Transfer for Power systems (IEEE Std C37.118.2™– 2011, revision of IEEE Std C37.118™-2005), December 2011.

[22] de la O Serna J.A., *Dynamic Phasor Estimates for Power System Oscillations*, IEEE Transaction on Instrumentation and Measurement, vol. 56, no. 5, 1648–1657 (2007).

[23] Platas-Garza M.A., de la O Serna J.A., *Dynamic Phasor and Frequency Estimates Through Maximally Flat Differentiators*, IEEE Transactions on Instrumentation and Measurement, vol. 59, no. 7, pp. 1803–1811, July (2010).

[24] de la O Serna J.A., Platas-Garza M.A., *Maximally flat differentiators through WLS Taylor decomposition*, Digital Signal Processing, vol. 21, Issue 2, pp. 183–194, March (2011).

[25] Nanda S., Dash P.K., *A Gauss-Newton ADALINE for a Dynamic Phasor Estimation of Power Signals and Its FPGA Implementation*, IEEE Transactions on Instrumentation and Measurement, vol. 67, no. 1, pp. 45–56, January (2018).

[26] Huang Ch., Xie X., Jiang H., *Dynamic Phasor Estimation Through DSTKF Under Transient Conditions*, IEEE Transactions on Instrumentation and Measurement, vol. 66, no. 11, pp. 2929–2936, November (2017).

[27] Rabe S., Komarnicki P., Styczynski Z.A., Gurbiel M., Blumschein J., Kereit M., Voropai N., *Automated Test Procedures for Accuracy Verification of Phasor Measurement Units*, 978-1-4673-2729-9/12, IEEE (2012).